Supplementary Information

A Skin-Adhesive Bimodal Sensing Patch for Decoding Occlusal Dysfunction

Longchao Huang[1, †], *Ruoxi Li*[2, †], *Xuelan Li*[1], *Yue Sun*[1], *Guanfa Li*[1], *Long Jin*[1], *Wei Zhu*[3, *], *Weiqing Yang*[1,4, *], *Weili Deng*[1, *]

[1] Key Laboratory of Advanced Technologies of Materials (Ministry of Education), School of Materials Science and Engineering, Southwest Jiaotong University, Chengdu 610031, P. R. China

[2] Institute of Biomedical Engineering College of Medicine, Southwest Jiaotong University, Chengdu 610031, P. R. China

[3] School of Energy and Power Engineering, Nanjing University of Science and Technology, Nanjing 210094, P. R. China

[4] Research Institute of Frontier Science, Southwest Jiaotong University, Chengdu 610031, P. R. China

[†] These authors contributed equally to this work

* Corresponding author: weili1812@swjtu.edu.cn; zhuwei@njust.edu.cn; wqyang@swjtu.edu.cn

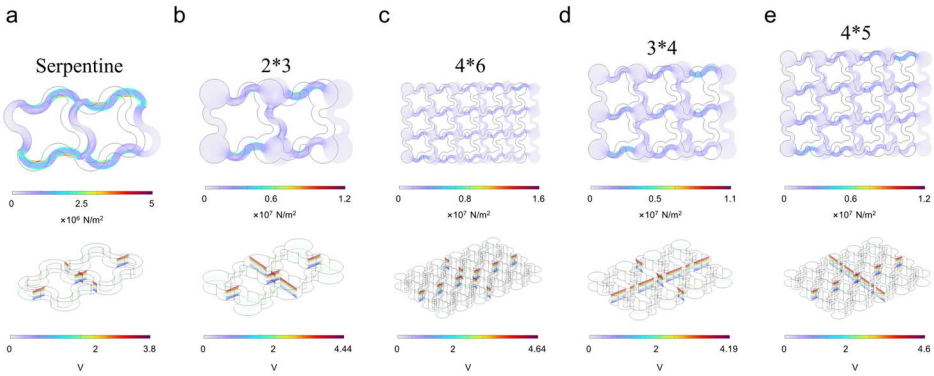

Figure S1. Stress distribution and piezoelectric response characteristics of serpentine PVDF films with different specifications under 40% strain.

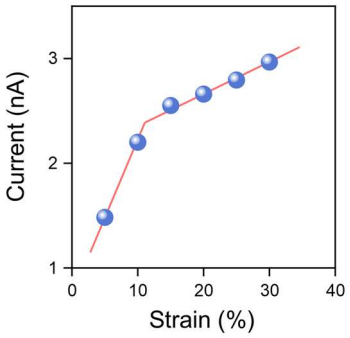

Figure S2. Piezoelectric current output of serpentine-structured PVDF film at 10 Hz under different strain ratios.

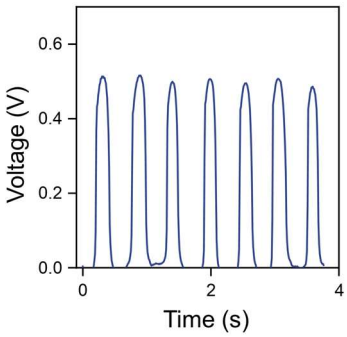

Figure S3. Piezoelectric voltage output of serpentine-structured PVDF film at 2 Hz under 30% strain ratio.

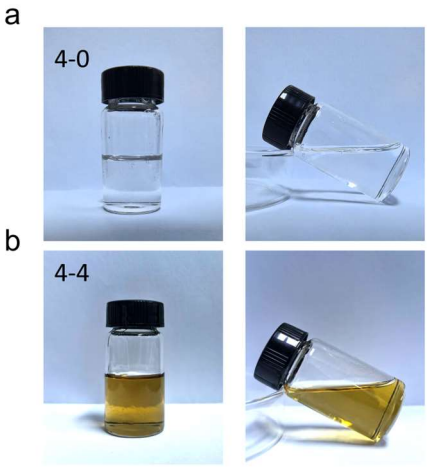

Figure S4. Digital photo of PT hydrogel ink.

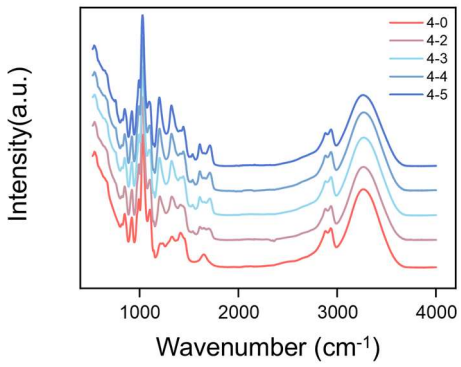

Figure S5. FTIR spectra of PT hydrogels with different TA contents.

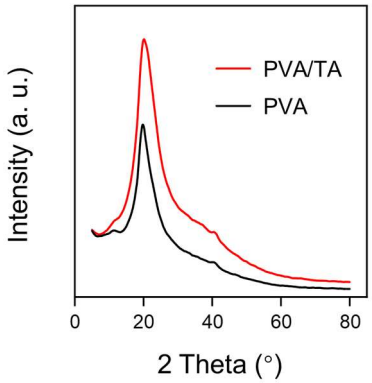

Figure S6. XRD Diffraction Patterns of PT Hydrogels with Different TA Contents.

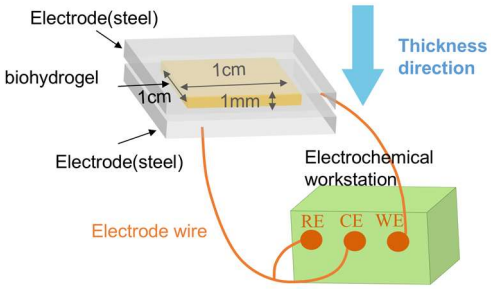

Figure S7. Schematic diagram of the interfacial impedance test for PT hydrogels.

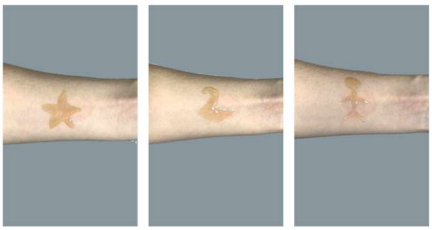

Figure S8. Digital photography of patterned PT hydrogels.

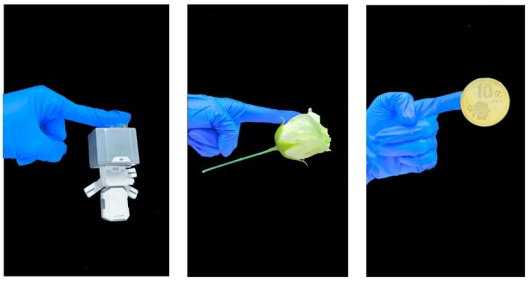

Figure S9. Digital photographs of PT hydrogels adhering to various objects as adhesives.

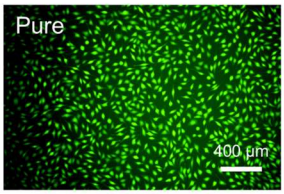

Figure S10. Biocompatibility testing of PT hydrogels.

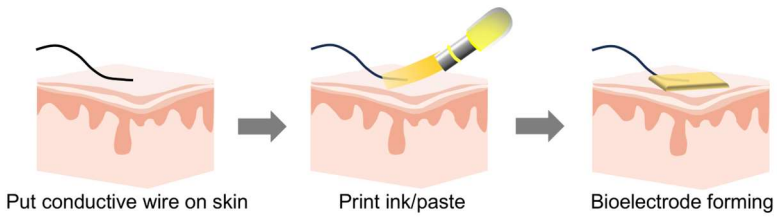

Figure S11. Schematic diagram of hydrogel as an electromyography electrode.

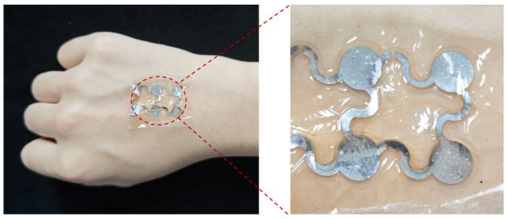

Figure S12. The hydrogel is applied as an adhesive to the skin surface, with a PVDF serpentine-structured film bonded on top, achieving conformal adhesion between the PVDF film and the skin surface.

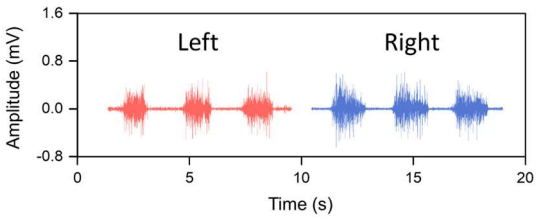

Figure S13. Electromyography of the left and right masseter muscles during mandibular deviation.

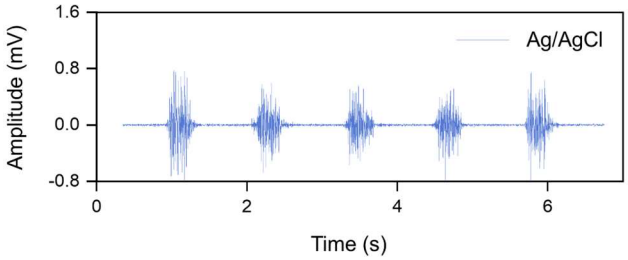

Figure S14. During normal occlusion, the EMG signals recorded by the commercial electrodes.

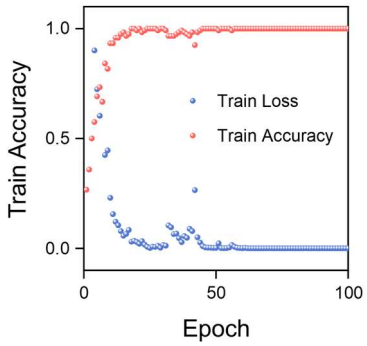

Figure S15. Classification accuracy and loss function of the multimodal training dataset over 100 epochs.

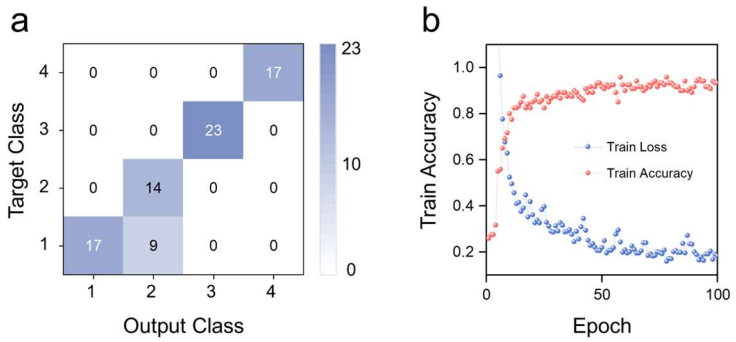

Figure S16. Piezoelectric sensor. (a) Confusion matrix. (b) Classification accuracy and loss function of the training dataset over 100 epochs.

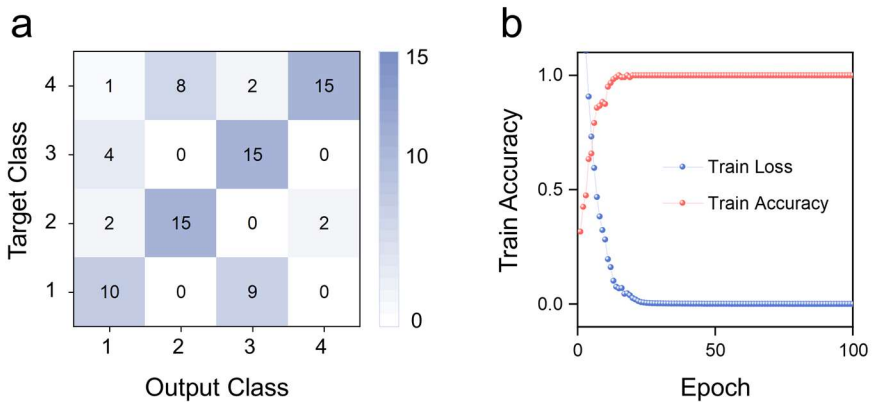

Figure S17. PT hydrogel EMG electrodes. (a) Confusion matrix. (b) Classification accuracy and loss function of the training dataset over 100 epochs.

Table S1. The composition of the PVA-TA biohydrogel with different solvents.

	PVA (g)	TA (g)	$AlCl_3 \cdot_6H_2O$ (g)	Glycerol(g)	Water/Ethanol	
1	1	1	0.2	3.97	5:4	√
2	1	1	0.2	3.97	4:5	√
3	1	1	0.2	3.97	3:6	×
4	1	1	0.2	3.97	2:7	×

Table S2. The composition of the PVA-TA biohydrogel with different TA content.

	4-0	4-2	4-3	4-4	4-5
PVA (g)	1	1	1	1	1
TA (g)	0	0.5	0.75	1	1.25